applied sciences

MDPI

Article

Investigating Blind Spot Design Effects on Drivers' Cognitive Load with Lane Changing: A Comparative Experiment with Multiple Types of Intelligent Vehicles

Xiaoye Cui †, Yijie Li †, Lishengsa Yue *, Haoyu Chen and Ziyou Zhou

Department of Transportation Engineering and Key Laboratory of Road and Traffic Engineering of Ministry of Education, Tongji University, Shanghai 201804, China; 2153616@tongji.edu.cn (X.C.); 2153613@tongji.edu.cn (Y.L.)
* Correspondence: 2014yuelishengsa@tongji.edu.cn
† These authors contributed equally to this work.

Abstract: Lane changing is a frequent traffic accident scenario. To improve the driving safety in lane changing scenarios, the blind spot display of lane changing is increased through human–machine interaction (HMI) interfaces in intelligent vehicles to improve the driver's rate of risk perception with regard to the driving environment. However, blind spot information will increase the cognitive load of drivers and lead to driving distraction. To quantify the coupling relationship between blind spot display and drivers' cognitive load, we proposed a method to quantify the cognitive load of the driver's interaction by improving the AttenD algorithm, collecting feature data by carrying out a variety of real-vehicle road-testing experiments on three kinds of intelligent vehicles, and then establishing a model blind spot design and driver cognitive load correlation model using Bayesian Logistic Ordinal Regression (BLOR) and Categorical Boosting (CatBoost). The results show that the blind spot image display can reduce the driver's cognitive load more effectively as it is closer to the driver, has a larger area, and occupies a higher proportion of the center control screen, especially when it is located in the middle and upper regions of the center control screen. The improved AttenD algorithm is able to quantify the cognitive load of the driver, which can be widely used in vehicle testing, HMI interface development and evaluation. In addition, the analytical framework constructed in this paper can help us to understand the complex impact of HMI in intelligent vehicles and provide optimization criteria for lane change blind spot design.

Keywords: intelligent vehicles; human–machine interaction design; driver cognitive load; blind spot design; lane-change safety; AttenD algorithm; smart cockpit

check for updates

Citation: Cui, X.; Li, Y.; Yue, L.; Chen, H.; Zhou, Z. Investigating Blind Spot Design Effects on Drivers' Cognitive Load with Lane Changing: A Comparative Experiment with Multiple Types of Intelligent Vehicles. *Appl. Sci.* **2024**, *14*, 7570. https://doi.org/10.3390/app14177570

Academic Editor: Suchao Xie

Received: 30 July 2024
Revised: 19 August 2024
Accepted: 23 August 2024
Published: 27 August 2024

Copyright: © 2024 by the authors. Licensee MDPI, Basel, Switzerland. This article is an open access article distributed under the terms and conditions of the Creative Commons Attribution (CC BY) license (https://creativecommons.org/licenses/by/4.0/).

1. Introduction

According to the World Health Organization's (WHO) statistical report on the risks to human life, road traffic accidents are now the eighth most common cause of death each year, with 19 million people per year dying in road accidents worldwide [1]. An analysis of the U.S. Highway Administration's traffic accident report shows that 90% of accidents are due to human factors [2], particularly high-risk events such as lane changes made by emergency vehicles. Statistics of accident data from 2010 to 2017 showed that serious accidents caused by emergency vehicles changing lanes accounted for up to 17% of the total number of accidents [3]. Studies have been conducted to analyze the causes of traffic accidents when changing lanes, and it was concluded that about 20% of accidents that occur while changing lanes are due to the driver having limited visibility [4]. The main reason for the high number of such accidents is the driver's failure or inability to adequately inspect their blind spot in a timely manner [5], and rearview mirrors alone cannot holographically perceive the risk [6]. It is true that many drivers perceive information about the traffic environment in their blind spot by looking around the vehicle to ensure a safe lane change. However, this practice distracts the driver's attention and increases the risk while driving [7]. In addition,

the duration of the lane change is very limited, and too many perceptual cues will increase the driver's cognitive load and increase the likelihood of unsafe driving behavior [8].

To raise awareness of the risks associated with driving, car manufacturers have implemented blind spot monitoring (BSM) systems that alert drivers to potential hazards when they are changing lanes. Studies have demonstrated that vehicles equipped with BSM systems are 14% less likely to be involved in lane-changing accidents compared to those without BSM systems [9]. With advancements in HMI interfaces, intelligent vehicles now display blind spot images when the turn signal is activated, aiding drivers in recognizing potential hazards in their blind spots during lane changes or turns, thereby mitigating accidents due to reduced visibility. However, the development of blind spot imaging technology remains rudimentary, lacking standardized design guidelines, resulting in considerable variability among car brands. User experience data indicate that the inadequate design of blind spot systems in current smart cars increases drivers' cognitive load and exacerbates distracted driving. Therefore, it is crucial to explore the mechanisms by which blind spot design influences drivers' cognitive load to provide a foundation for the advancement of intelligent vehicle technologies.

A major challenge in this research is to measure and quantify the cognitive load of drivers without disturbing them while they are driving on real roads. There are various methods for measuring cognitive load, which have been discussed in detail in previous studies [10]. Among the methods commonly used to assess cognitive load, subjective and physiological measures predominate. Subjective measures usually rely on questionnaire responses that reflect drivers' perceptions to measure the extent of their cognitive load (e.g., NASA Task Load Index [11] and Subjective Workload Assessment Technique [12] scales). In contrast, physiological measures assess cognitive load by measuring physiological indicators such as respiratory rate [13,14], pupil diameter [15,16], cardiovascular activity [14,17,18], and brain activity [19–22]. Although subjective measurements are simple and easy to perform, the accuracy of their results is often compromised due to individual differences in the interpretation and perception of rating scales. Physiological measures provide greater accuracy in representing cognitive load but are intrusive, making them impractical for in-vehicle road testing in this study as the equipment required to record electroencephalogram and electrocardiogram signals would interfere with driving. Therefore, it is critical to choose a system for measuring and quantifying cognitive load that does not hinder drivers in complex real-world driving environments and whose ability to reflect drivers' mental load is not compromised. Given the correlation between lane change accidents and drivers' visual search patterns [23], we would also like to see a method of measuring cognitive load that correlates with drivers' gaze positions. Such an approach would not only facilitate its wide application in various tests on real roads but would also allow monitoring of drivers' interactions with their forward vision, rearview mirrors, and blind spot images during lane changes in different directions. This would improve the evaluation of the relationship between drivers' cognitive load and blind spot design.

An increase in cognitive load manifests itself in particular in increased distraction while driving: the higher the cognitive load, the worse the driving performance [24], accompanied by corresponding changes in the driver's visual characteristics [25,26], which usually leads to more hazardous situations or accidents. The research by Melnicuk et al. [27] also shows that increase in cognitive load impairs driving performance, especially lateral control of the vehicle, implying an increased risk of driving accidents. Currently, there is a research gap in analyzing the effects of blind spot images on driver cognitive load, although numerous studies have investigated the degree of driver distraction. As early as 2004, Barkana et al. [28] used a loss of fixation analysis to qualify the distracting effect of cell phone conversations on the visual field. In recent years, more and more researchers have explored better methods and mechanisms to quantify driver distraction [29,30]. This research has progressively addressed various scenarios, including lane changes, turning, and responses to emergencies. For example, Xu et al. [31] used an embedding kernel

algorithm to detect critical mismatched driver visual attention during lane changing and evaluate the safety of driver behavior during lane changing. Although many studies have investigated driver distraction during lane changing, few have analyzed the effects of blind spot images on driving safety during lane changing in intelligent vehicles. In addition, there are few studies that establish correlation models between driver cognitive load and vehicle types and blind spot location. Mekata et al. [32] compared the cognitive load and mental stress of drivers in a driving simulator when the side-rear wide-angle monitor was placed in different positions and showed that positioning the monitor in the middle of the driver minimized cognitive load and facilitated information intake. Nevertheless, no relevant model was created in this study to analyze the factors influencing cognitive load, and driving simulators cannot fully replicate real driving conditions. There is, therefore, an urgent need for research to close this gap in this area.

To develop a quantitative method for measuring cognitive load that minimizes driver distraction and reflects the dynamic changes in the visual interaction domain during lane changes, while using the computed cognitive load to build models for analyzing the effects of blind spot design, traffic environment, and other factors on driver cognitive load, we propose an improved AttenD algorithm capable of dynamically adjusting driving-related domains. By integrating experimental data from real vehicles that reflect authentic road traffic conditions, we build relevant models to analyze the extent of various factors affecting driver cognitive load. The main contributions of this study are as follows:

1. We refine the AttenD algorithm to accurately capture the driver's attention during lane changes based on the improved algorithm.

2. We propose a blind spot assessment method to design blind spots, including the size and location of the blind spot, in a way that reduces the cognitive load on the driver.

The remainder of this paper is organized as follows: Section 2 introduces the methodology. Section 3 explains the experimental design and data collection process. Section 4 presents the results of the study. Section 5 discusses the results and then presents the conclusions.

2. Methodology

We aim to investigate the effects of blind spot image display design and other environmental factors on driver cognitive load in lane changing scenarios of intelligent vehicles. The flowchart of this study is shown in Figure 1.

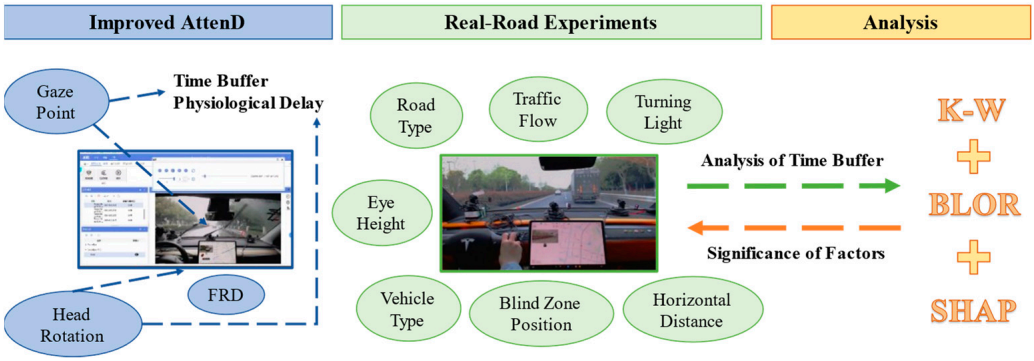


Figure 1. The flowchart of methodology.

Firstly, we establish a relationship model between drivers' visual buffer value and fixation points to quantify their cognitive load in real-vehicle experiments. Correlation statistical analysis is then conducted between the experimental results and variables.

Subsequently, Bayesian Logistic Ordinal Regression (BLOR) is utilized to further ascertain the correlation between drivers' cognitive load and factors such as fixation height, traffic flow, road type, blind spot distance, vehicle type, and lane-changing direction.

Furthermore, to decipher the influence of each feature on drivers' cognitive load, we integrate the Categorical Boosting (CatBoost) and SHapley Additive exPlanations (SHAP) models to construct an interpretability framework assessment.

2.1. Experiments

To collect data on the effect of lane changing processed blind spot design on drivers' cognitive load, we conduct real-world road tests based on three types of intelligent vehicles to fully document the driver's performance data during lane changing. There are significant differences among the three vehicle models in terms of the size and aspect ratio of the central control screen, the size and aspect ratio of the blind spot image, the position of the blind spot image, and the blind spot image proportion of the central control screen. These differences are conducive to exploring the impact of different blind spot image design parameters on drivers' cognitive load. Additionally, the blind spot positions in two of the types are adjustable, while in the remaining type, the blind spot image positions corresponding to the left and right turn signals are different. Under otherwise identical conditions, this allows us to study the impact of blind spot position and lane changing on cognitive load.

The experiment is divided into two sections: The first involves conducting separate tests on three different vehicle brands to comprehensively analyze the impact of various variables, including blind spot design, the driver's gaze height, the road and traffic environment, and the lane-changing direction, on driver cognitive load. The second involves altering the position of the blind spot to observe changes in driver cognitive load. The target time period for the experiment covers the entire process of the driver completing the lane-changing behavior, starting from turning on the turn signal and ending with turning it off. The collected data include eye-tracking metrics such as gaze height, fixation point location, fixation duration, and fixation frequency, as well as other information such as road traffic flow level and road type.

2.2. Algorithm for Cognitive Load Calculation

The AttenD algorithm is used to detect the driver's level of distraction and can quantify the driver's cognitive load based on eye movement data. Its basic assumption is that human attention is closely linked to gaze behavior. It also introduces the concept of a time buffer to reflect the driver's cognitive load [33]. When the driver's gaze frequently deviates from the driving-relevant region (FRD), the time buffer value decreases, indicating increased cognitive load. In other words, the time buffer value is negatively correlated with the extent of the driver's cognitive load.

In existing studies, the FRD in the AttenD algorithm is usually considered to be fixed. However, in reality, there are differences in the size and location of these regions from driver to driver or lane change direction. Therefore, in this study, by observing the swipe pattern and gaze characteristics of each driver, based on which the range of FRD coordinates was selected when changing lanes to the left or right, we improved the AttenD algorithm by varying the FRD dynamically to make the results of the cognitive load calculation more accurate.

Figure 2 illustrates the process framework of the improved AttenD algorithm, which was implemented using the R programming language. The detailed procedure is as follows:

The key thresholds and parameters for judging the driving load are provided at first, including an initial value of 2.0 s for the time buffer value, an initial physiological response delay of 0 s with a threshold of 0.1 s, an initial delay for the rearview mirror and central control screen of 0 s with a threshold of 1.0 s, and a time step of 0.0167 s. Then, we input the integrated and cleaned dataset, read each data entry, and calculate the time buffer value according to the following steps.

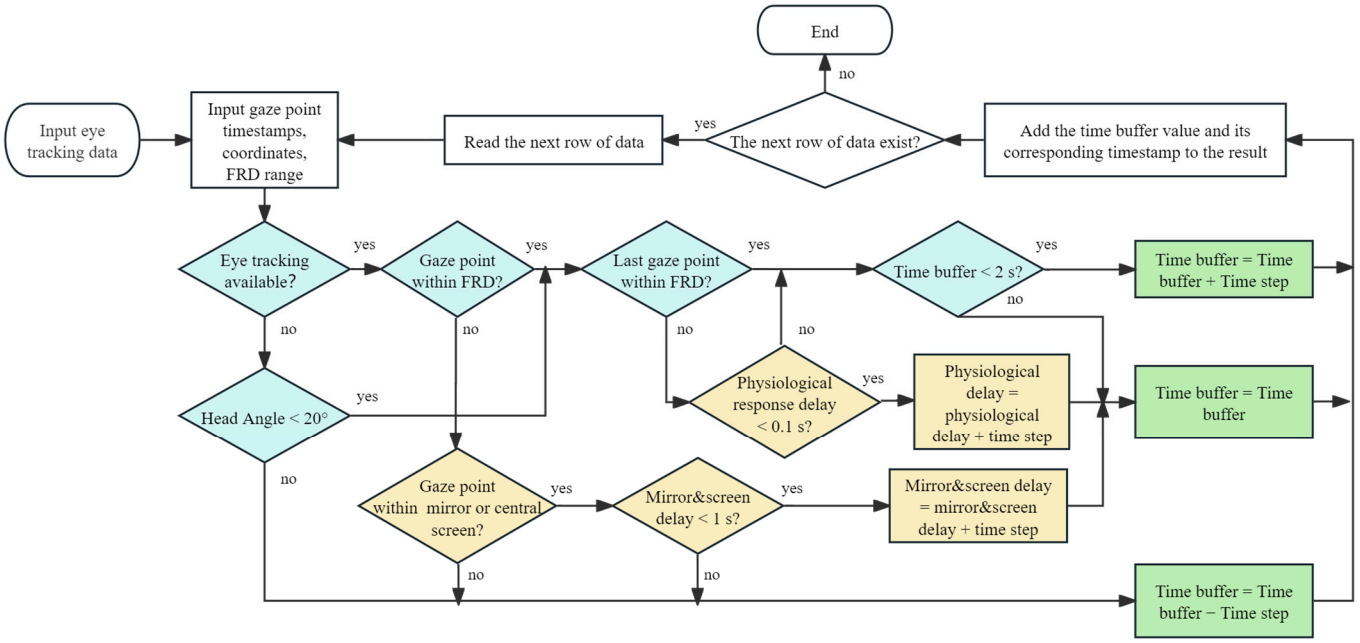


Figure 2. Flowchart of the improved AttenD algorithm.

Step 1: Match the corresponding FRD region according to the driver behavior (left lane change or right lane change) corresponding to each gaze point. If the value of gaze point quality is higher than the threshold value, the eye movement indicator is considered valid and it is time to progress to step 3; if it is lower than the threshold value, switch to the head rotation angle indicator and go to step 2.

Step 2: If the head rotation angle is greater than or equal to 20°, output the time buffer value as the time buffer minus the actual time step length; if it is less than 20°, consider that both the gaze point at the current timestamp and the previous timestamp are within the FRD and proceed to step 3.

Step 3: If both of the current and the previous timestamps are within the FRD, judge the result of the output time buffer value; otherwise, go to step 4. If the time buffer value is equal to 2 s, the output time buffer value is equal to the original. If the time buffer value is less than 2 s, the output time buffer value is the original time buffer value plus the time step.

Step 4: If the gaze point of the current timestamp is within the FRD but the previous one is not, make a judgment based on the physiological response delay value; otherwise, go to step 5. If the physiological response delay is less than 0.1 s, update the physiological response delay value to the physiological response delay value plus the time step, and the time buffer value will remain unchanged. If it is greater than or equal to 0.1 s, then the time buffer value is calculated in the same way as in step 3.

Step 5: If the viewpoint of the current timestamp is not within the FRD, the evaluation is based on other driving-related regions. If the viewpoint is neither in the rearview mirror nor in the dashboard, the output time buffer value is the original time buffer value minus the time step. If the viewpoint is in the rearview mirror or the dashboard and the delay between the rearview mirror and the central control screen is less than the threshold value, the value of updating the delay between the rearview mirror and the central control screen is the original value plus the time step, and the output time buffer value remains unchanged; if the delay exceeds the threshold value, the output time buffer value is the original time buffer value minus the time step.

After iterating through the entire data table, generate an integrated results table that maps each timestamp to its corresponding time buffer value.

2.3. Impact Analysis Model

To analyze the effects of the feature variables on driver cognitive load, we performed correlation analysis, statistical analysis, and machine learning modeling. We identified the key variables that influence driver cognitive load in lane change scenarios and clarified the coupling relationship between these factors and driver cognitive load to provide a basis for designing blind spot images. Then, we discretized the variable time buffer value into ordered levels and used it as an explanatory variable with the different feature factors as explanatory independent variables to construct a mechanistic analysis model.

2.3.1. Kruskal–Wallis Test

The Kruskal–Wallis test serves as a commonly employed nonparametric method for examining whether two or more samples originate from the same probability distribution. We implemented it using SPSS (Statistical Package for the Social Scienc-es, version 26.0.0.0, IBM). In the statistical process, all sample data are ranked in ascending order, and the test statistic H is calculated using Equation (1):

$$H = \frac{12}{N(N+1)} \sum_{i=1}^{k} \frac{R_i^2}{n_i} - 3(N+1) \tag{1}$$

where N represents the total sample size, k is the number of groups, and R_i denotes the sum of ranks in the ith group.

In statistics, the p-value is frequently employed to indicate the asymptotic significance of the test statistic. Given that the test statistic H approximately follows a chi-square distribution with $k-1$ degrees of freedom, the cumulative distribution function (CDF) of the chi-square distribution is utilized to compute the p-value (p) using Equation (2):

$$p = 1 - \mathrm{CDF}_{\chi^2}\ (H, k-1) \tag{2}$$

2.3.2. Bayesian Logistic Ordinal Regression

Compared to traditional logistic regression models, the Bayesian Logistic Ordinal Regression model has three major advantages: first, it is well suited for analyzing the logistic regression relationship between ordered categorical explanatory variables and multiple types of dependent variables; second, Bayesian estimation of the model parameters can handle the uncertainty of the parameters better than maximum likelihood estimation; and third, Bayesian estimation integrates the prior distributions with the likelihood function of the data to derive the posterior distribution of the model parameters, which reflects the probability distribution of the parameters after observing the data and allows for more robust and comprehensive statistical inference. Therefore, this study builds a model for the relationship between cognitive load and other variables of the scene to analyze the effects of various factors on drivers' cognitive load [34,35].

The utility function of the Bayesian ordered logit regression model is expressed as Equation (3) [36]:

$$l_{ij} = \boldsymbol{x}_{\boldsymbol{ij}}^{\boldsymbol{T}}\boldsymbol{\beta} + \boldsymbol{b_i} + \varepsilon_{ij} \tag{3}$$

where i represents the feature variable and j denotes the number of experimental units for each feature variable.

$\boldsymbol{x}_{\boldsymbol{ij}}^{\boldsymbol{T}}$ represents the i*j matrix formed by the feature variables and the number of experiments, which is associated with the fixed effect parameter vector $\boldsymbol{\beta}$ of the dimension. $\boldsymbol{b_i}$ is a random effect and ε_{ij} is a logically distributed error term, with its distribution function being calculated in Equation (4):

$$f(\varepsilon_{ij}) = \frac{e^{-\varepsilon_{ij}}}{\left(1+e^{-\varepsilon_{ij}}\right)^2} \tag{4}$$

Since l_{ij} is unobservable, it can be indirectly measured through the observable ordered variable y_{ij}. Therefore, y_{ij} can be defined as Equation (5):

$$y_{ij} = \begin{cases} 1 & if\ -\infty < l_{ij} < \gamma_1, \\ 2 & if\ \gamma_1 < l_{ij} < \gamma_2, \\ \vdots & \vdots \\ C & if\ \gamma_{C-1} < l_{ij} < \infty \end{cases} \tag{5}$$

where γ_c represents the boundary between intervals corresponding to the observed outcomes, as shown in Equation (6).

$$\gamma^T = (\gamma_{min} < \gamma_1 < \cdots < \gamma_{C-1} < \gamma_{max}), \text{with } \gamma_{min} = -\infty, \gamma_{max} = \infty \tag{6}$$

In the model, we focus on the cumulative probabilities, such as the probability that $y \leq \gamma_c$. Based on the distribution of ε, the cumulative response probability for the c category of the ordinal outcome y_{ij} is calculated using Equation (7).

$$\begin{aligned} P(y_{ij} \leq \gamma_c | \boldsymbol{\beta}, \boldsymbol{b}) &= \pi_{ij(c)} = P(l_{ij} \leq \gamma_c | \boldsymbol{\beta}, \boldsymbol{b}) \\ &= P\left(\boldsymbol{x_{ij}^T \beta} + \boldsymbol{b_i} + \varepsilon_{ij} \leq \gamma_c\right) \\ &= P\left(\varepsilon_{ij} \leq \gamma_c - \boldsymbol{x_{ij}^T \beta} - \boldsymbol{b_i}\right) \\ &= \frac{exp\left(\gamma_c - \boldsymbol{x_{ij}^T \beta} - \boldsymbol{b_i}\right)}{1 + exp\left(\gamma_c - \boldsymbol{x_{ij}^T \beta} - \boldsymbol{b_i}\right)}, \\ &for\ \ c = 1, 2, \ldots, C-1. \end{aligned} \tag{7}$$

This can be formulated as a cumulative logit model included in Equation (8):

$$log\left(\frac{\pi_{ij(c)}}{1 - \pi_{ij(c)}}\right) = \gamma_c - \ \boldsymbol{x_{ij}^T \beta} - \boldsymbol{b_i}, \quad for\ c = 1, 2, \ldots, C-1. \tag{8}$$

Using the inverse link for this model, we can calculate $P(y = c|\boldsymbol{\beta}, \boldsymbol{b}) = \pi_{ij(c)}$ in Equation (9):

$$\pi_{ij(c)} = P(\gamma_{c-1} < l_{ij} < \gamma_c) = \frac{exp\left(\gamma_c - \boldsymbol{x_{ij}^T \beta} - \boldsymbol{b_i}\right)}{1 + exp\left(\gamma_c - \boldsymbol{x_{ij}^T \beta} - \boldsymbol{b_i}\right)} - \frac{exp\left(\gamma_{c-1} - \boldsymbol{x_{ij}^T \beta} - \boldsymbol{b_i}\right)}{1 + exp\left(\gamma_c - \boldsymbol{x_{ij}^T \beta} - \boldsymbol{b_i}\right)} \tag{9}$$

Then, the joint posterior density of the parameter vector and latent variable becomes Equation (10):

$$P\left(\boldsymbol{\beta}, \boldsymbol{\gamma}, \boldsymbol{b}, \sigma_{\beta}^2, \sigma_{\boldsymbol{b}}^2, \boldsymbol{l} \,/\, \boldsymbol{y}\right) \propto\ P(\boldsymbol{y}/\ \boldsymbol{l}, \boldsymbol{\gamma})\ P(\ \boldsymbol{l}/\ \boldsymbol{\beta}, \boldsymbol{b})\ P(\boldsymbol{\gamma}) \times P\left(\boldsymbol{\beta}\ /\sigma_{\beta}^2\right)\ P\left(\ \boldsymbol{b}\ /\sigma_{\boldsymbol{b}}^2\right)\ P\left(\sigma_{\beta}^2\right)\ P\left(\sigma_{\boldsymbol{b}}^2\right) \tag{10}$$

The prior for the $C-1$ unknown thresholds has been given as order statistics from $U(\gamma_{min}, \gamma_{max})$ distribution using Equation (11) [37]:

$$P(\boldsymbol{\gamma}) = (C-1)!\left(\frac{1}{\gamma_{max} - \gamma_{min}}\right)^{C-1} I(\boldsymbol{\gamma} \in T) \tag{11}$$

where $T = \{(\gamma_1, \ldots, \gamma_{max}) | \gamma_{min} < \gamma_1 < \cdots < \gamma_{C-1} < \gamma_{max}\}$.

The posterior conditional distribution of $\boldsymbol{\beta}$ is defined by Equation (12)

$$\boldsymbol{\beta}|ELSE\ \sim N_p\left(\widetilde{\boldsymbol{\beta}}_0, \widetilde{\boldsymbol{\Sigma}}_0\right) \tag{12}$$

where

$$\widetilde{\boldsymbol{\Sigma}}_0 = \left(\boldsymbol{\Sigma}_0^{-1}\sigma_\beta^{-2} + \boldsymbol{X}^T\boldsymbol{D}_\omega\boldsymbol{X}\right)^{-1},$$

$$\widetilde{\boldsymbol{\beta}}_0 = \widetilde{\boldsymbol{\Sigma}}_0\left(\boldsymbol{\Sigma}_0^{-1}\sigma_\beta^{-2}\boldsymbol{\beta}_0 - \boldsymbol{X}^T\boldsymbol{D}_\omega Zb + \boldsymbol{X}^T\boldsymbol{D}_\omega l\right).$$

with

$$l = \left[l_1^T, \ldots, l_I^T\right]^T, l_i = \left[l_{i1}^T, \ldots, l_{in_i}^T\right]^T,$$

$$X = \left[X_1^T, \ldots, X_I^T\right]^T, X_i = \left[x_{i1}, \ldots, x_{in_i}\right]^T$$

$$Z = \begin{bmatrix} \boldsymbol{l}_{n_1} & \boldsymbol{0} & \cdots & \boldsymbol{0} \\ \boldsymbol{0} & \boldsymbol{l}_{n_2} & \cdots & \boldsymbol{0} \\ \vdots & \vdots & \ddots & \vdots \\ \boldsymbol{0} & \boldsymbol{0} & \cdots & \boldsymbol{l}_{n_1} \end{bmatrix}, \boldsymbol{D}_\omega = diag(\boldsymbol{D}_{\omega 1}, \ldots, \boldsymbol{D}_{\omega I})$$

$$\boldsymbol{D}_\omega = diag(\boldsymbol{D}_{\omega 1}, \ldots, \boldsymbol{D}_{\omega I}),$$

$$\boldsymbol{D}_{\omega i} = diag(\omega_{i1}, \ldots, \omega_{in_i}).$$

Equation (12) indicates that, given the data (denoted as *ELSE*), the posterior distribution of the regression coefficient $\boldsymbol{\beta}$ is a multivariate normal distribution with mean $\widetilde{\boldsymbol{\beta}}_0$. The mean $\widetilde{\boldsymbol{\beta}}_0$ and the covariance matrix $\widetilde{\boldsymbol{\Sigma}}_0$ are determined jointly by the prior covariance, observed data, and corresponding weighting information. This allows the estimates of the regression coefficients to be dynamically adjusted based on the observed data, providing a more accurate reflection of the model's response to the data.

2.3.3. Categorical Boosting

Due to the assumption of independence and identical distribution between the variables in the ordered logit model, the direct application of this model in our study faces a challenge, as the time buffer values come from multiple driving tasks of 15 drivers, leading to substantial correlations between the data samples that are hardly compatible with the assumption of independence and identical distribution. To solve this problem, we introduce the nonparametric and learning-based CatBoost (Categorical Boosting) method for further analysis. We also use SHAP (SHapley Additive exPlanations) [38–40] to interpret the results of the machine learning approach and gain insights into the predictions of the model.

The data used in this study primarily comprise categorical variables with a small proportion of numerical variables and thus represent extensive high-dimensional data. The CatBoost algorithm incorporates an innovative approach that automatically converts categorical features into numerical features. In addition, the algorithm uses combinatorial categorical features that enable the discovery of relationships between features, which significantly enriches the structure and hierarchy of the feature space. Due to these properties, the CatBoost algorithm is used to analyze the relationship [41,42].

The output formula of CatBoost is shown in Equation (13):

$$\hat{x}_k^i = \frac{\sum_{j=1}^{p-1}\left[x_{\sigma_{j,k}} = x_{\sigma_{p,k}}\right]Y_{\sigma_j} + a \times p}{\sum_{j=1}^{p-1}\left[x_{\sigma_{j,k}} = x_{\sigma_{p,k}}\right] + a} \tag{13}$$

where $\hat{x}_k^i$ represents the predicted value for feature k and category i;

Y_{σ_j} represents the target value (label) for sample j;

p represents the added prior distribution term;

a is typically a positive weight coefficient.

SHapley Additive exPlanations (SHAP) is a methodology for interpreting the results of machine learning models. Based on game theory, a prediction model outputs a predicted value for a specific person. The SHAP method assumes that each feature makes a "contribution" to the target prediction and assigns it a Shapley value to quantify its importance.

The sum of the Shapley values of all characteristics for a particular person corresponds to the target prediction, with adjustments made for the average predicted value. We adopt Tree SHAP for feature importance analysis.

The Shapley value represents the average marginal contribution of a particular feature i to the prediction. For a model with n features, the Shapley value of each feature is calculated using Equation (14) [43]:

$$\Phi_i(v) = \sum_{S \in N} \frac{[(|S|-1)!(n-|S|)!]}{n!} \times [v(s) - v(s \backslash \{i\})] \quad (14)$$

where $\Phi_i(v)$ represents the Shapley value of feature i;

N is the set of all features;

S is any subset of N that does not contain feature i;

$v(S)$ denotes the contribution of the feature set (S) to the model's output.

A key property of SHAP values is additivity, meaning that the sum of SHAP values across all features equals the model's output. For a given prediction model $f(x)$, its output can be expressed as Equation (15):

$$f(x) = \Phi_0 + \sum_{i=1}^{n} \Phi_i \quad (15)$$

where Φ_0 is the model's output at the baseline value, while Φ_i is the SHAP value of feature i.

3. Data Collection

3.1. Overview of Experiments

In our experiment, we used the SmartEye Pro eye-tracking system (version 10.2.0, Noldus, Sweden) to capture the visual behavior of drivers interacting with blind spot images during lane changes. The system is equipped with three infrared cameras and an additional supplementary camera. It calculates the line-of-sight direction by measuring the vector between the pupil center and the corneal reflection reference point, which is produced using an active infrared light source. Head rotation angles are obtained from the head pose captured by the cameras, and the height of the eyes is recorded in real time from the camera images. The data are then synthesized using HRT (Human Research Tool) software (version 1.6.0, INFO instrument, Shanghai, China), which includes a foreground wide-angle camera, to merge the driver's foreground video with the line-of-sight direction data and determine the driver's point of gaze coordinates.

For the first set of experiments (Experiment 1), a total of 15 drivers with experience in smart car driving and the habit of observing their blind zone image during lane changing were recruited and divided into three groups, with each group driving the same vehicle model. Three vehicle types with significant differences in the blind zone image designs chosen are shown in Figure 3. The experimental route (Figure 4) spanned approximately 38.5 km, with each test lasting roughly 90 min. The route was designed with numerous turns to prompt drivers to perform autonomous lane changes.



Figure 3. Three types of vehicles used in experiment 1 (from **left** to **right**: Type 1, Type 2, Type 3).

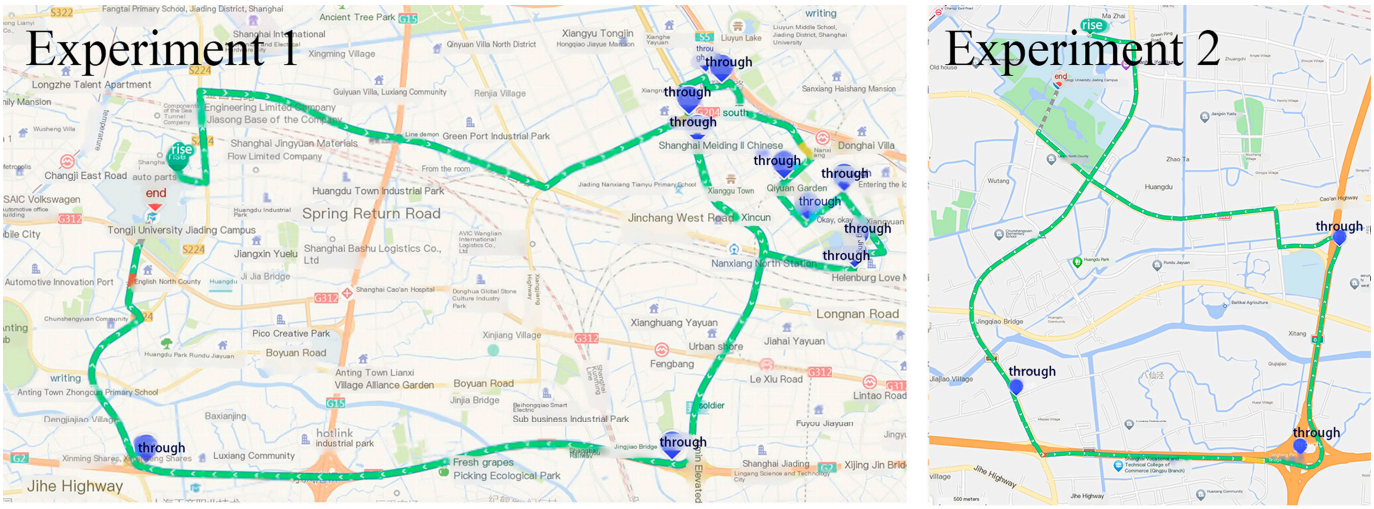


Figure 4. The route for Experiment 1 and Experiment 2.

For the second set of experiments (Experiment 2), nine drivers with similar backgrounds were recruited, each of whom completed three driving trials using a vehicle of Type 1 with different blind zone image positions, as the blind zone image of Type 1 can be dragged to three positions as shown in Figure 5. Each trial covered approximately 15 km and lasted about 20 min (Figure 4). To mitigate the influence of experimental sequence on drivers' cognitive load variations, the order of blind zone image positions varied for each driver during the experiments.



Figure 5. Three blind zone positions of Vehicle Type 1 in Experiment 2 (from **left** to **right**: position 1, position 2, and position 3).

3.2. Experimental Data

The experiments employed the SmartEye Pro eye-tracking system to capture the visual behaviors of drivers interacting with blind spot images during lane changing. This system is equipped with four gaze-tracking cameras, which capture the dynamic gaze of the drivers, while a foreground wide-angle camera records the frontal scenery during driving. Utilizing the accompanying Human Research Tool (HRT) software, the foreground video and gaze data of the drivers are synthesized to obtain metrics such as fixation points, gaze heights, and head rotation angles. The data collected from the two sets of experiments are encompassed in Table 1, and detailed information about traffic flow levels and vehicle parameters is shown in Figure 6, Tables 2 and 3.

Table 1. Indicators of the collected data.

Indicator	Explanations
Gaze Landing Point Coordinates	Taking the upper left corner of the HRT's foreground video as the origin, the horizontal and vertical pixel distances corresponding to the driver's gaze are output. These are used in the calculation of the time buffer value within the AttenD algorithm.
Head Rotation Angle	The left–right head rotation angles captured by the eye-tracker, which serve as auxiliary data for the calculation of the time buffer value.
Eye Height	The z-axis coordinate of the driver's gaze origin position, as output by the eye-tracker in the world coordinate system.
Traffic Flow Level	Based on the volume of vehicles ahead on the road, traffic flow is classified into three levels: high, medium, and low. An example of traffic flow levels is illustrated in Figure 7.
Road Type	The type of road where the vehicle was located during data collection, categorized as city roads or expressways.
Lane Change Direction	The direction of lane change (left or right) corresponding to each data entry.
Vehicle Type	As mentioned in Section 4.1, the vehicle type was analyzed as an overall variable to examine its impact on cognitive load in Experiment 1. Relevant parameters of the three vehicle types are presented in Table 2, where ρ represents the ratio of the blind zone image to the center screen and D represents the horizontal distance from the left end of the blind zone image to the center of the steering wheel.
Blind Zone Image Position	As mentioned in Section 4.1, three positions of blind zone images of the first type of vehicles are selected for further experiments to analyze the influence of the blind zone image positions on the driver's cognitive load. Relevant parameters of the three positions are presented in Table 3, where D represents the horizontal distance from the left end of the blind zone image to the center of the steering wheel, D1 represents the distance from the left end of the blind zone image to the left of the center screen, and D2 represents the distance from the top of the blind zone image to the top of the center screen.
Horizontal Distance of the Left End of the Blind Zone Image from the Center of the Steering Wheel	Since the distance of the blind spot from the driver's eyes is positively correlated with its distance from the center of the steering wheel, and the driver's head will rotate to a certain extent during the driving process, it is difficult to measure the distance from the eyes to the blind spot directly. Therefore, this study measured the distance from the left end of the blind spot to the center of the steering wheel, which was combined with the height of the driver's line of sight to reflect the effect of the distance from the driver's eyes to the blind spot on the driver's cognitive load. Relevant parameters have been listed in Tables 2 and 3.

Table 2. Parameters of center screen and blind zone image of the selected vehicle types.

Vehicle Type	Center Screen			Blind Zone Image			ρ	D/cm
	Length /cm	Width /cm	Area /cm^2	Length /cm	Width /cm	Area /cm^2		
1	33.1	20.7	685.2	12	6.1	73.2	0.11	21.2
2	65.8	10.9	717.2	L: 10.9	9.0	L: 98.1	L: 0.14	L: −14.5
				R: 16.0		R: 144.0	R: 0.20	R: 34.2
3	21.8	23.9	521	12.2	7.2	87.8	0.17	38.0



Figure 6. Different levels of traffic flow.

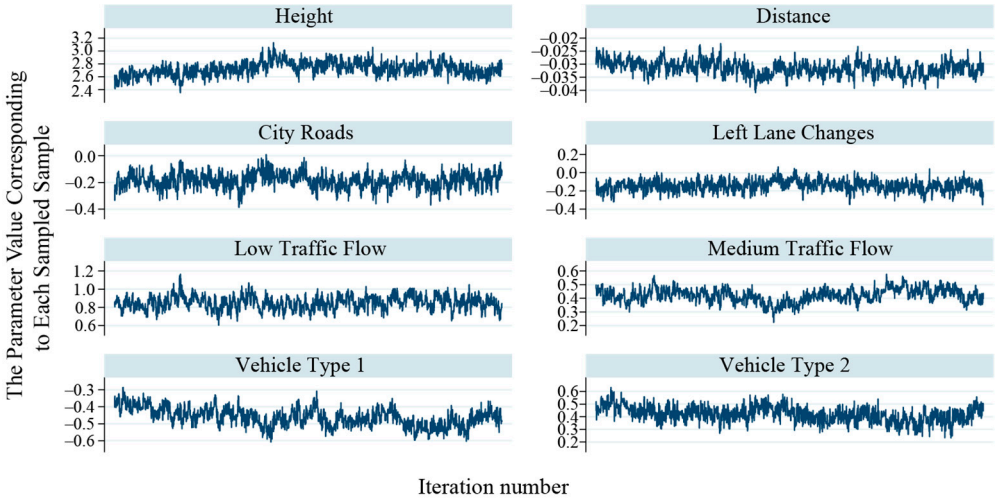


Figure 7. MCMC sampling trace plots of Experiment 1.

Table 3. Detailed parameters of the blind spot image for different positions of Vehicle Type 1.

Vehicle Type	Position	D/cm	D1/cm	D2/cm
1	1	21.2	0.3	3.5
	2	34.2	13.3	1.0
	3	21.2	0.3	12.7

3.3. Data Preprocessing

The experimental dataset is divided into two parts: Raw eye movement data recorded at 60 frames per second and recordings of feature variables at each lane change. The raw eye movement data are converted into a time buffer value for each frame using the AttenD algorithm. We used the coordinates of the driver's gaze points for each frame to filter out the time buffer data when the driver's gaze fell into the blind spot. These values were then matched with other feature variables using timestamps. Each data entry represents the moment the driver looked into the blind spot and the corresponding status. The time buffer values were evenly categorized into three levels: "low", "medium", and "high", based on their numerical magnitude.

4. Results and Discussions

4.1. Descriptive Statistical Analysis

The descriptive statistical analysis section of this study aims to preliminarily investigate the correlation among automobile brands, blind spot locations, and drivers' cognitive load, as well as the variations in drivers' cognitive load levels under different lane-changing scenarios. For Experiment 1, the mean and standard deviation of the time buffer values corresponding to each vehicle type in each lane-changing scenario were calculated, and a Kruskal–Wallis test was conducted to obtain the *p*-values between vehicle types and their respective mean and standard deviation values. For Experiment 2, the mean and standard deviation of the time buffer values corresponding to each blind spot location in each lane-changing scenario were computed, and a Kruskal–Wallis test was employed to determine the *p*-values between blind spot locations and their respective mean and standard deviation values.

4.1.1. Descriptive Statistical Analysis of Experiment 1

The nonparametric statistical results for each traffic scenario in Experiment 1 are presented in Table 4. Regarding the traffic flow level, due to the insufficient sample size in the low traffic flow scenario, only the high and medium traffic flow scenarios are analyzed in this section.

Table 4. Nonparametric statistical results for different traffic scenarios in Experiment 1.

	p-Value of Veh-Mean	*p*-Value of Veh-Std.	Vehicle Type	Veh-Mean	Veh-Std.	Mean	Std.
City Roads	0.471	0.501	1	1.363	0.556	1.379	0.577
			2	1.368	0.665		
			3	1.406	0.511		
Expressway	0.026	0.041	1	1.522	0.438	1.685	0.326
			2	1.828	0.214		
			3	1.705	0.326		
Right Lane Changes	0.282	0.366	1	1.343	0.561	1.410	0.557
			2	1.389	0.634		
			3	1.497	0.476		
Left Lane Changes	0.309	0.506	1	1.508	0.459	1.594	0.383
			2	1.798	0.26		
			3	1.477	0.43		
Medium Traffic Flow	0.014	0.02	1	1.538	0.421	1.500	0.465
			2	1.77	0.278		
			3	1.191	0.697		
High Traffic Flow	0.096	0.226	1	1.156	0.699	1.347	0.602
			2	1.278	0.739		
			3	1.606	0.367		

The results indicate that the mean values of time buffer values are generally smaller in city road (mean—city roads = 1.379; mean—expressway = 1.685), right lane change (mean—right lane changes = 1.410; mean—left lane changes = 1.594), and high traffic flow (mean—medium traffic flow =1.500; mean—high traffic flow = 1.347) scenarios, representative of the higher cognitive load. In the expressway (p = 0.026) and medium traffic flow (p = 0.014) scenarios, vehicle types have a significant correlation with the time buffer values, which means vehicle types have a strong impact on drivers' cognitive load in these two scenarios. In contrast, the influence of vehicle types on driver cognitive load is not evident for both lane-changing directions.

Comparing the mean and standard deviation of the time buffer values corresponding to different vehicle types in the traffic environments with strong correlation between vehicle types and time buffer values, it is found that the time buffer values corresponding to Type 2 have the largest mean value and the smallest standard deviation, which is judged to be the blind zone design that best meets the sweeping characteristics of the driver when changing lanes and results in a lower cognitive load. Conversely, Type 1 exhibits the smallest mean time buffer value, corresponding to the highest cognitive load on drivers.

4.1.2. Descriptive Statistical Analysis of Experiment 2

The nonparametric statistics for each traffic scenario in Experiment 2 are shown in Table 5. It is found that there is a significant correlation between the blind spot locations and the time buffer values under the three traffic scenarios of expressway (p = 0.014), left lane change (p = 0.012), and high traffic (p = 0.003), which indicates that the blind spot locations have a relatively large effect on the cognitive load of the drivers in these three traffic scenarios.

Table 5. Nonparametric statistical results for different traffic scenarios of Experiment 2.

	p-Value of Veh-Mean	*p*-Value of Veh-Std.	Position	Veh-Mean	Veh-Std.
City Roads	0.197	0.294	1	1.391	0.548
			2	1.534	0.424
			3	1.344	0.563
Expressway	0.014	0.02	1	1.601	0.395
			2	1.684	0.355
			3	1.317	0.597
Right Lane Changes	0.208	0.165	1	1.418	0.533
			2	1.443	0.464
			3	1.191	0.661
Left Lane Changes	0.012	0.082	1	1.483	0.478
			2	1.725	0.338
			3	1.472	0.494
Low Traffic Flow	0.477	0.473	1	1.37	0.547
			2	1.543	0.401
			3	1.081	0.738
Medium Traffic Flow	0.918	0.95	1	1.587	0.404
			2	1.585	0.405
			3	1.592	0.387
High Traffic Flow	0.003	0.009	1	1.35	0.583
			2	1.618	0.388
			3	1.357	0.574

By comparing the mean and standard deviation of the time buffer values in different traffic environments, it is found that the blind spot image at position 3 has the smallest mean and largest standard deviation of the time buffer value, which is considered to have the largest cognitive load on the driver. The cognitive load is smallest when the blind spot image is at position 2 and is slightly higher at position 1. This pattern only shows anomalies under medium traffic, with high probability caused by a poor correlation.

4.2. Bayesian Logistic Ordinal Regressions

4.2.1. Results and Analysis of Experiment 1

Due to the complex and multidimensional nature of the posterior distribution in Bayesian Logistic Ordinal Regression, it is quite difficult to obtain an analytical solution directly. To estimate the parameters effectively, researchers have applied the Markov Chain Monte Carlo (MCMC) method. MCMC is an algorithm commonly used for sampling of complex probability distributions. By calculating statistical quantities such as the mean, variance, and 95% confidence interval of the posterior distribution, the results represent estimates of the fixed effects. The model underwent a total of 12,500 MCMC iterations, with the first 2500 iterations discarded as a burn-in phase and the remaining 10,000 iterations forming the final MCMC sample set. The acceptance rate (AR) was 0.21, meaning that 21% of the 10,000 estimated parameter values were accepted. An AR of over 10% indicates that there are no problems with the convergence of the MCMC, confirming the validity of the model.

In Figure 7, the sample values in the MCMC sampling trace plots fluctuate randomly without showing an upward or downward trend. Overlapping trajectories from multiple chains indicate consistent sampling results across different chains. The samples in the trace plots exhibit good mixing in the parameter space, with frequent fluctuations. The samples do not linger near a particular value for extended periods. After the warm-up phase, the trace plots display a stable distribution. The vertical axis in the figure represents the parameter value corresponding to each sample. The concentration of values above zero indicates that the respective feature factor has a positive effect on increasing the time buffer, thereby reducing the driver's cognitive load. Conversely, values distributed below zero suggest that the feature factor increases the driver's cognitive load. Based on this analysis, we can preliminarily conclude that a higher eye height, low traffic flow, medium traffic flow, and Vehicle Type 2 all contribute to reducing the driver's cognitive load. On the other hand, a longer distance and Vehicle Type 1 both increase the driver's cognitive load. Meanwhile, the effects of city roads and left lane changes are not evident. As shown in Table 6, the BLOC estimates include the posterior mean, posterior standard deviation (Std. dev.), MCMC standard error (MCSE), posterior median, and 95% credit interval. Among the characteristic variables in this model, except for drivers' eye height, the MCSE values for all others are less than 0.01, indicating low variability across repeated simulations and, thus, reliable results. The close proximity of the posterior means to the medians for all characteristic variables suggests that the posterior distributions are approximately normal. Furthermore, the fact that the 95% credit intervals for all characteristic factors exclude zero demonstrates a statistically significant correlation between each factor and driver cognitive load.

Table 6. BLOC estimation table of Experiment 1.

	Mean	Std. Dev.	MCSE	Median	[95% Cred. Interval]	
Eye Height	2.388	0.402	0.055	2.388	1.586	3.142
Distance	−0.030	0.003	0.000	−0.030	−0.037	−0.023
City Roads	−0.203	0.051	0.004	−0.203	−0.302	−0.104
Left Lane Changes	0.152	0.056	0.003	0.151	0.043	0.266
Low Traffic Flow	0.839	0.075	0.009	0.838	0.687	0.987
Medium Traffic Flow	0.419	0.054	0.006	0.420	0.302	0.520
Vehicle Type 1	−0.409	0.097	0.009	-0.410	−0.602	−0.221
Vehicle Type 2	0.429	0.087	0.006	0.431	0.259	0.595

In this table, expressway, right lane changes, high traffic flow and Vehicle Type 3 are omitted.

In Table 6, "omitted" represents the benchmark value for comparison. A negative fixed effect indicates a higher probability of reducing the time buffer, implying an increased cognitive load for drivers, while a positive effect suggests the opposite. The analysis of the results is as follows:

1. Driver Behavior:

The driver's eye height exhibits a strong positive correlation with the time buffer (mean = 2.388042 > 0, 95% CI 1.59 to 3.14), suggesting that within a certain range, a higher eye height is associated with a lower cognitive load. This is presumed to stem from a broader field of vision when the line of sight is higher in a range [44].

2. Traffic Environment:

On city roads, the probability of increased cognitive load for drivers is higher under identical scenarios (mean = −0.203 < 0). City roads are often constrained by multiple physical obstacles such as buildings, street trees, and traffic facilities, leading to a compressed field of vision for drivers. This limitation not only complicates the perception of potential

hazards but also necessitates more frequent adjustments in gaze and attention to allow drivers to comprehensively assess and respond to dynamic changes in their surroundings. Additionally, the complexity of city road environments, with pedestrians, non-motorized vehicles, various types of motor vehicles, and intricate traffic signals and signs, contributes significantly to the cognitive load of drivers.

Left-lane changing reduces the cognitive load of drivers by 15%, compared to right-lane changing scenarios. Given that blind spot information is concentrated in the driver's right field of view, the driver focuses mainly on the forward area of the target lane during left-lane changing. Consequently, blind spot alerts from the right (non-focal side) are more likely to capture the driver's attention. In right-lane-changing scenarios, the spatial overlap of blind spot images and the driving task (observing the right lane conditions) along the line of sight can create a "redundant information" effect, potentially leading to an increase in the cognitive load. In addition, since the driver's seat is located on the left, the road information required when changing to the right lane is farther away from the driver, which is also one of the possible factors that can cause a higher cognitive load.

Compared to high traffic flow, medium traffic flow reduces drivers' cognitive load by 84%, while low traffic flow reduces it by 42%, indicating that lower-traffic environments are more likely to decrease cognitive load. In high traffic flow, the density and rate of information change significantly increase, demanding numerous and complex decisions from drivers within short timeframes, thereby heightening the burden on their cognitive systems. Conversely, in low-traffic flow, with fewer road users, the volume and complexity of information decrease, substantially reducing the information processing required by drivers and alleviating cognitive pressure.

3. Blind Spot Imaging Design:

The distance between the blind spot image and the steering wheel center is negatively correlated with the time buffer (mean = -0.03, 95% CI -0.04 to 0.02), suggesting that within a certain range, positioning the blind spot image closer to the steering wheel center is more likely to reduce drivers' cognitive load.

Comparing the blind spot imaging designs of Vehicle Type 2 and Vehicle Type 3, Vehicle Type 2's design is more effective in reducing drivers' cognitive load (mean = 0.43 > 0, 95% CI 0.26 to 0.60). Vehicle Type 2 boasts a larger display area for blind spot images on the center console, closer to the driver, facilitating information capture.

When comparing Vehicle Type 3 and Vehicle Type 1, Vehicle Type 3's design also outperforms that of Vehicle Type 1 when it comes to reducing drivers' cognitive load (mean = -0.41, 95% CI -0.60 to 0.22). Although Vehicle Type 3's blind spot images are farther from the driver, the larger display area and higher proportion of blind spot images on the center console likely outweigh this distance factor, resulting in a net reduction in cognitive load.

In summary, among various vehicle blind spot image designs, those featuring larger display areas for blind spot images on the center console and a higher proportion of such images are more likely to reduce drivers' cognitive load.

4.2.2. Results and Analysis of Experiment 2

To avoid the problem of imbalanced data, in this section, the medium traffic flow is merged into the low-traffic-flow category for comparative analysis with the high traffic flow. The model ran a total of 12,500 MCMC iterations, with the initial 2500 iterations considered as the burn-in phase and discarded, leaving the remaining 10,000 iterations to constitute the final MCMC sample set. The acceptance rate (AR) was 0.22, indicating that 22% of the 10,000 estimated parameter values were accepted. An AR above 10% suggests that there are no issues with the convergence of MCMC, validating the model's effectiveness.

Similar to Experiment 1, the sampling trace plots (Figure 8) in Experiment 2 exhibit random fluctuations, stable distributions, and are within a reasonable range of temporal buffer values. Upon preliminary analysis of the sampled parameter values in Figure 8, it is observed that the intervals of various feature variables all encompass the value of 0, suggesting that these variables do not exhibit a pronounced effect on the driver's cognitive load.

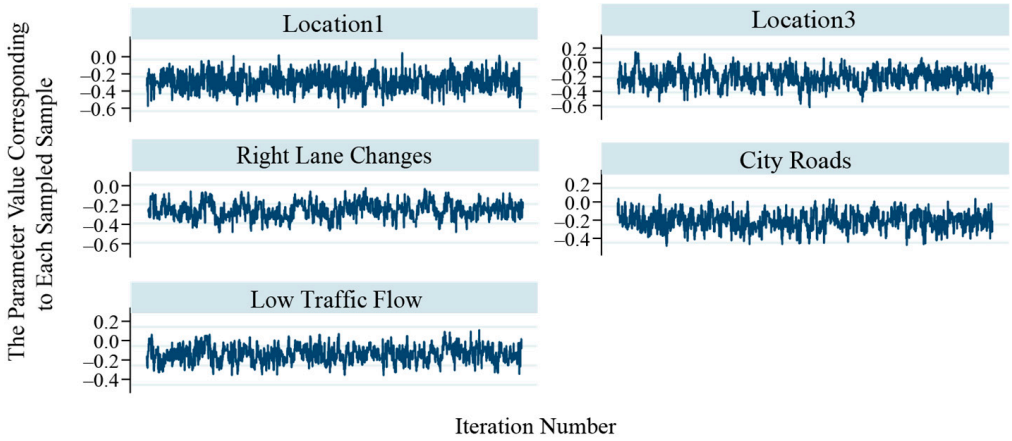


Figure 8. MCMC sampling trace plots of Experiment 2.

As shown in Table 7, within this model, the MCSE values for all feature variables were less than 0.01, indicating a low variability in the simulated results of MCMC across different replications, thus rendering the results relatively reliable. Furthermore, the posterior means and medians of all feature variables were very close, suggesting that the posterior distributions approximated normal distributions.

Table 7. BLOC estimation table of Experiment 2.

	Mean	Std. Dev.	MCSE	Median	[95% Cred. Interval]	
Location1	−0.234	0.090	0.010	−0.234	−0.398	−0.053
Location3	−0.188	0.095	0.006	−0.189	−0.373	0.007
Right Lane Changes	−0.254	0.081	0.009	−0.255	−0.405	−0.083
City Roads	−0.150	0.091	0.008	−0.149	−0.330	0.033
Low Traffic Flow	−0.082	0.078	0.004	−0.084	−0.230	0.081

In this table, expressway, right lane changes, high traffic flow and Vehicle Type 3 are omitted.

The analysis of the results is as follows:

(1) Traffic Environment: The conclusions regarding lane-changing direction and road type align with those of Experiment 1, validating the effectiveness of the analytical results from Experiment 1.

(2) Blind Spot Location: comparing position 1 (mean = −0.23, 95% CI −0.39 to 0.05) with the same longitudinal position but a different transverse position with position 2 (omitted), the latter shows a greater potential to reduce the cognitive load of drivers. Furthermore, when position 1 (with the above mean and confidence interval) is compared with position 3 (mean = −0.18, 95% confidence interval −0.37 to 0.01), which has the same transverse position but a different longitudinal position, position 3 shows a more pronounced effect in reducing drivers' cognitive load. However, the confidence interval of position 3 includes 0, which means that the correlation is not statistically significant. The displayed blind spot image is located near the driver's lateral distance and at the same longitudinal position. Positioning the blind spot display closer to the geometric center of the central display can reduce the driver's cognitive load more effectively.

4.3. Impact Factor Analysiss

4.3.1. The Effect of Individual Characteristic Factors on Cognitive Load

The average absolute value of the SHAP value indicates the degree of influence of that feature on cognitive load, with a larger value suggesting a greater impact on cognitive load. A feature density scatter plot is plotted as shown in Figures 9 and 10:

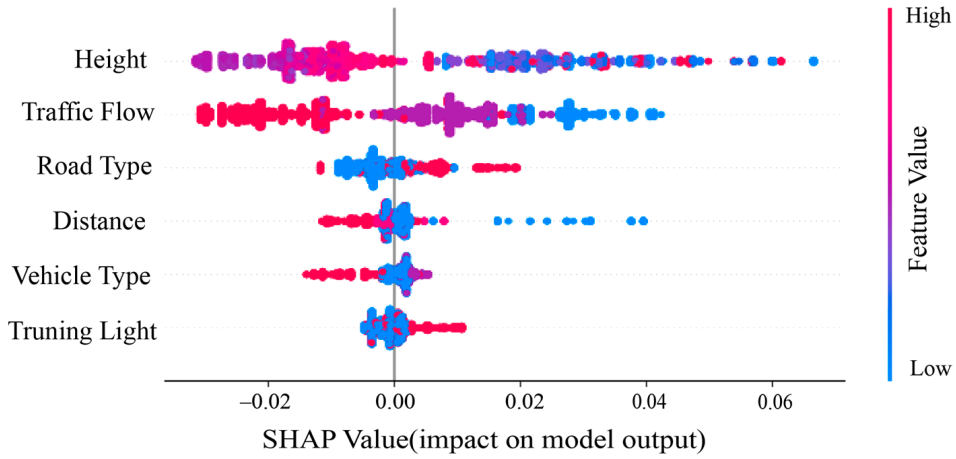


Figure 9. Feature density scatter plots for Experiment 1.

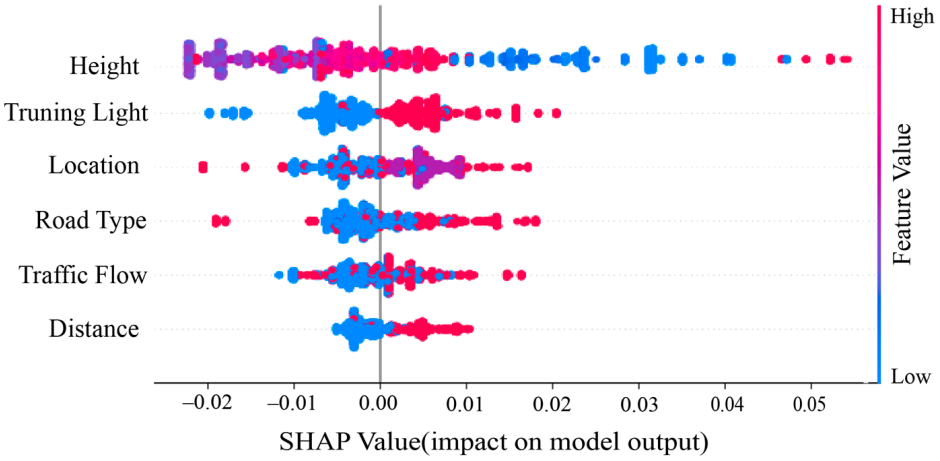


Figure 10. Feature density scatter plots for Experiment 2.

As depicted in the figure, each row represents a feature factor. The horizontal axis corresponds to the SHAP value for each sample of that factor. A positive SHAP value indicates a positive impact on the time buffer, which translates to reduced cognitive load; a negative SHAP value indicates the opposite. The color of the sample points indicates the magnitude of the feature itself, with redder colors representing higher values and bluer colors representing lower values. The analysis of the results is as follows:

1. Vehicle Type:

Most points for the vehicle type feature fall near SHAP = 0, indicating a minimal impact on cognitive load. The blind spot imaging design of Brand 3 has a negative impact on cognitive load, potentially due to the excessively long vertical length of the central display screen.

2. Blind Spot Design Features:

Blind spot design is divided into two parts. Firstly, the position of the blind spot image, represented by the distance and location indicators, shows a positive correlation between distance and time buffer, suggesting that a shorter distance between the blind spot and the

steering wheel center results in a lower cognitive load within a certain range. This could be attributed to a shorter scanning path for drivers to quickly capture the blind spot image and retrieve information, resulting in a lower cognitive load. The correlation between location and time buffer is significant, with Location 2 positively correlated and Location 1 negatively correlated, indicating that Location 2 reduces driver cognitive load compared to Location 1, consistent with previous analysis. The SHAP values for Location 3 are evenly distributed on both sides of 0, indicating no significant impact on driver cognitive load. Secondly, the size of the blind spot image and its proportion of the central display screen are determined by the vehicle type, which, according to Analysis (1), has an insignificant impact on cognitive load. However, Brand 3 displays different blind spot images during left and right lane changes, necessitating further analysis.

3. Environmental Factors:

Overall, traffic environmental factors align with BLOR results: the traffic flow is negatively correlated with the time buffer, indicating increased cognitive load with higher traffic flow; left lane changes show a significant positive correlation with the time buffer, while right lane changes show the opposite, suggesting reduced cognitive load during left lane changes compared to right lane changes; expressways positively correlate with the time buffer, while urban roads have limited correlation with cognitive load, indicating a potential reduction in driver cognitive load on expressways.

4. Driver Characteristics:

Sample points representing higher eye heights are concentrated near 0, indicating minimal impact on cognitive load when drivers have higher eye heights. Conversely, lower eye heights significantly impact drivers' cognitive load.

4.3.2. Interaction Effects

To calculate the SHAP values under the interaction of multiple variables, we focus on analyzing the combined influence of blind spot image features and other factors.

As shown in Figure 11, the horizontal axis represents the eye height, and the vertical axis represents the SHAP value for eye height. The color of the sample points indicates three different vehicle brands, where the vehicle type can reflect characteristics such as the size of the blind spot image design and its proportion on the central display screen. It is evident from the figure that drivers in Vehicle Type 1 have a relatively higher eye height, with most sample points distributed above 0.7, while drivers in Vehicle Types 2 and 3 have a lower eye height, which may be related to the design of the driver's seat. When the eye height approaches 0.8, it negatively impacts the cognitive load, with Brand 1 showing a stronger negative correlation between blind spot image height and cognitive load. This could be attributed to its shorter vertical central display screen and smaller proportion of blind spot image display, making eye height have a more significant impact on the driver's ability to capture information. Conversely, when the eye height is lower or higher, the cognitive load positively correlates with eye height, with Brands 1 and 3 exhibiting stronger positive correlations than Brand 2, suggesting that a longer vertical height of the central display screen is more likely to induce changes in the driver's cognitive load.

As depicted in Figure 12, the SHAP values for all brands under the right lane change scenario are concentrated between -0.004 and 0.002, indicating a minimal influence of vehicle type on driver cognitive load in this scenario. In contrast, Brand 2 is more likely to reduce driver cognitive load during left lane changes compared to Brand 3, as Brand 2 provides more accessible information when a blind spot appears on the left side during left lane changes. This finding is not contradictory to previous discussions on lane change directions, since the spatial overlap between the blind spot image and the left rearview mirror during left lane changes is low, and they do not share the same line of sight.

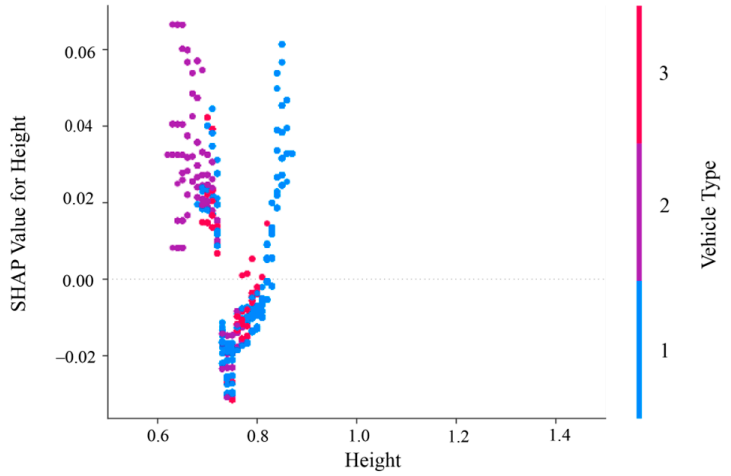


Figure 11. Height–vehicle type dependence scatter plot.

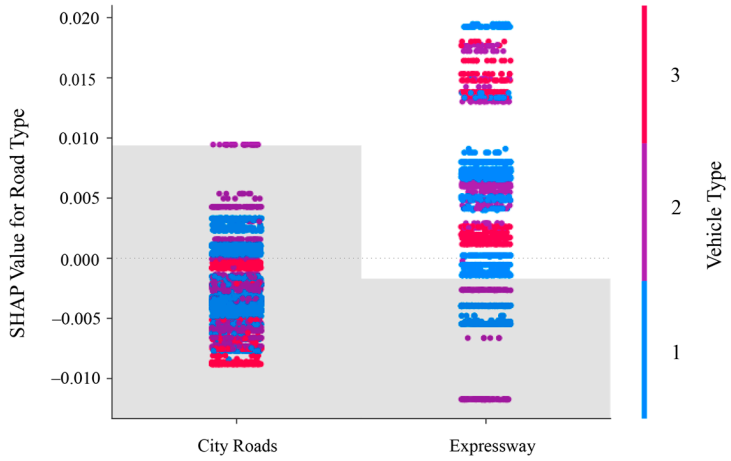


Figure 12. Road Type–Vehicle type dependence scatter plot.

Figure 13 illustrates that Position 3 positively affects driver cognitive load under low traffic flow but negatively impacts it under high traffic flow. This is speculated to be due to Position 3's blind spot image being prone to obstruction. Under low traffic flow, drivers can easily observe the blind spot image in time, but under high traffic flow, its vulnerability to obstruction hinders timely observation, leading to increased driver cognitive load.

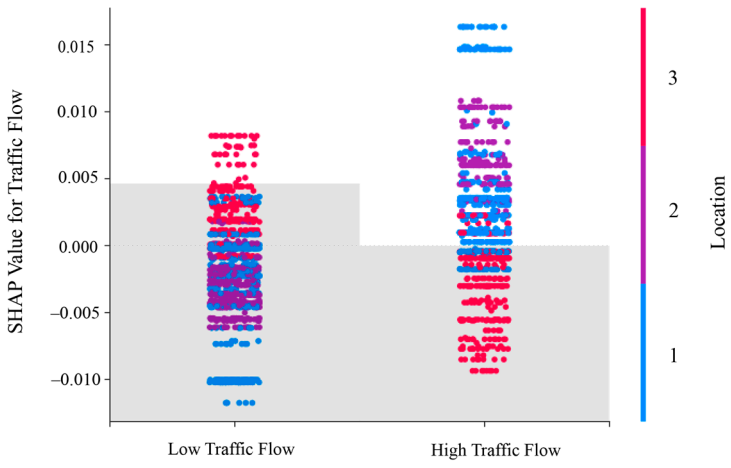


Figure 13. Traffic flow–location dependence scatter plot.

Figure 14 shows a stark contrast in Position 3's impact based on the direction of lane changes. During right lane changes, the SHAP values are concentrated between −0.015 and −0.02, indicating an increased likelihood of cognitive load. In contrast, during left lane changes, the SHAP values are between 0.005 and 0.02, suggesting a reduced cognitive load. This may be attributed to the ease of capturing information in Position 3 when simultaneously observing the rearview mirror and blind spot during left lane changes, which involves a larger scanning range.

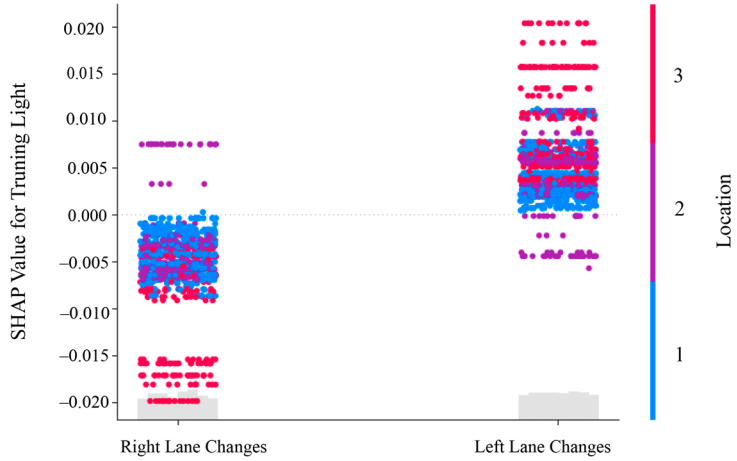


Figure 14. Traffic flow–location dependence scatter plot.

Figure 15 demonstrates that Position 2, with a larger distance between the blind spot and the central display screen, has SHAP values concentrated above 0, while Positions 1 and 3, with shorter distances, have SHAP values concentrated below 0. This suggests that Position 2 is more likely to effectively reduce drivers' cognitive load compared to Positions 1 and 3, which is consistent with previous analyses.

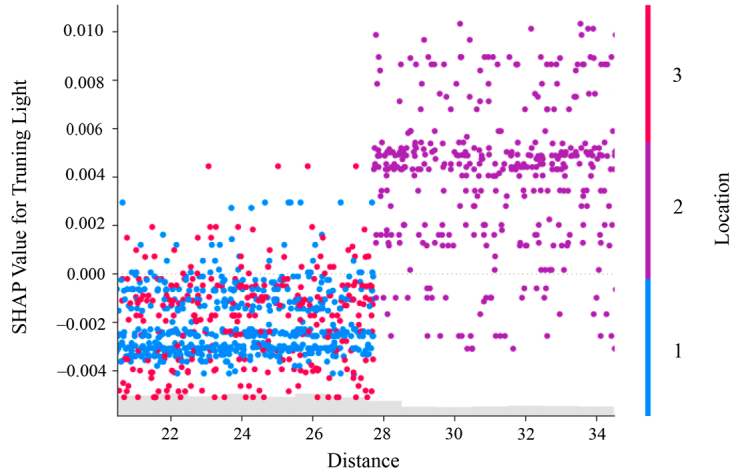


Figure 15. Traffic flow–location dependence scatter plot.

5. Conclusions

The objective of this study was to quantify the relationship between blind spot display and drivers' cognitive load during lane changing in intelligent vehicles. To achieve this, an improved AttenD algorithm was developed to measure the cognitive load, and various real-vehicle road-testing experiments were conducted to gather data. Subsequently, a correlation model between blind spot design and driver cognitive load was established using BLOR and CatBoost. The detailed conclusions are as follows:

(1) In terms of the design of the blind spot image display's size ratio, increasing the size of the central display screen, the area designated for blind spot image display, and the proportion of the blind spot image on the central display screen can effectively assist drivers in acquiring blind spot image information, thereby reducing cognitive load during lane changes.

(2) Regarding the position of the blind spot image display, the more closely the blind spot image is displayed to the driver and positioned in the upper-middle section of the central control screen, the more effectively it can reduce the driver's cognitive load.

(3) Sight height and traffic environment also have an impact on the cognitive load of the driver. Within a certain range, there is a strong positive correlation between the collision buffer time value and the driver's line-of-sight height. The lower the line-of-sight height, the greater the impact on the driver's cognitive load.

Compared to previous research on blind spot monitoring systems or cognitive load, this paper offers the following innovations:

(1) This study is forward-looking, focusing on the design of blind spot images on central control screens, an area that has been widely implemented in modern intelligent vehicles but lacks sufficient research. This provides a new direction for the study of human–machine interaction safety in intelligent vehicles.

(2) The real-vehicle road testing method employed in this project not only produces experimental data that more accurately reflect real driving conditions but also allows for the control of variables, which enables a comparison of how the design features of blind spot images in different vehicle models impact drivers' cognitive load. This approach is superior to previous studies that evaluated driving safety solely through accident data [9] or driving simulator experiments [15].

(3) Based on data analysis, this paper establishes two models with high goodness-of-fit to analyze the factors and mechanisms affecting cognitive load. Compared to studies that only perform statistical analysis [32], this paper provides a more reliable explanation of the factors influencing cognitive load.

By altering the experimental conditions, our methods can also be applied to investigate the impact of other visual or auditory information on driver cognitive load during driving, including the design of traditional rearview mirrors, radio adjustments, and the voice control functions in modern intelligent vehicles.

Although this study investigated the impact of blind spot design on drivers' cognitive load, the research had some limitations. On the one hand, this study overlooked the effect of drivers' habits on cognitive load, potentially leading to individual differences in the research conclusions. On the other hand, since Type 1 vehicles allow for blind spot position adjustments in only three locations, exploring the global optimal solution for these positions poses certain challenges. In future research, we will continue to investigate the impact of blind spot position changes in other vehicle models on driver cognitive load, establish corresponding mathematical models between blind spot position parameters and time-to-collision buffer values, and develop an evaluation system for assessing the quality of blind spot image designs to assist automakers in optimizing turn signal blind spot image designs.

Author Contributions: Conceptualization, X.C., Y.L. and L.Y.; methodology, X.C. and L.Y.; software, X.C. and H.C.; validation, Y.L. and X.C.; formal analysis, X.C. and Y.L.; investigation, L.Y., X.C., Y.L., H.C. and Z.Z.; resources, L.Y.; data curation, X.C., Y.L. and Z.Z.; writing—original draft preparation, Y.L. and X.C.; writing—review and editing, L.Y.; visualization, X.C. and Y.L.; supervision, L.Y.; project administration, L.Y.; funding acquisition, L.Y. All authors have read and agreed to the published version of the manuscript.

Funding: This research was funded by the National Natural Science Foundation Project under Grant 52302442.

Institutional Review Board Statement: This study was approved by the Institutional Ethics Committee of Tongji University for studies involving humans with the approval number tjdxsro80 on 15 April 2024.

Informed Consent Statement: Informed consent was obtained from all subjects involved in the study.

Data Availability Statement: The data presented in this study are available on request from the corresponding author. Due to confidentiality agreements, access to the raw data may be restricted.

Acknowledgments: The College of Transportation and Engineering of Tongji University provided all the equipment we need. Our sincere gratitude goes to our college and all the volunteers who actively participated in this research.

Conflicts of Interest: The authors declare no conflict of interest. The funders had no role in the design of the study; in the collection, analyses, or interpretation of data; in the writing of the manuscript, or in the decision to publish the results.

References

1. Václaviková, I.; Holienková, J.; Selecká, L. Global status report on road safety 2023. In *Health and Safety*; World Health Organization: Geneva, Switzerland, 2023; pp. 15–16.
2. Zhang, T.; Chan, A.H.S. The association between driving anger and driving outcomes: A meta-analysis of evidence from the past twenty years. *Accid. Anal. Prev.* **2016**, *90*, 50–62. [CrossRef] [PubMed]
3. Shawky, M. Factors affecting lane change crashes. *IATSS Res.* **2020**, *44*, 155–161. [CrossRef]
4. Piccinini, G.; Simoes, A.; Rodrigues, C. Focusing on Drivers' Opinions and Road Safety Impact of Blind Spot Information System (BLIS). In *Advances in Human Aspects of Road and Rail Transportation*; CRC Press: Boca Raton, FL, USA, 2013; pp. 57–66.
5. Hargis, E. Blind Spot Accidents: Everything You Need to Know. Available online: https://www.lilawyer.com/blog/blind-spot-accidents/ (accessed on 10 April 2024).
6. Hatamleh, H.; Sharadqeh, A.A.M.; Alnaser, A.a.M.; Alheyasat, O.; Abu-Ein, A.A.-K. Computer Simulation to Detect the Blind Spots in Automobiles. *Int. J. Comput. Sci. Issues* **2013**, *10*, 453–456.
7. Chun, J.; Lee, I.; Park, G.; Seo, J.; Choi, S.; Han, S.H. Efficacy of haptic blind spot warnings applied through a steering wheel or a seatbelt. *Transp. Res. Part F Psychol. Behav.* **2013**, *21*, 231–241. [CrossRef]
8. Fitch, G.M.; Lee, S.E.; Klauer, S.; Hankey, J.; Sudweeks, J.; Dingus, T. *Analysis of Lane-Change Crashes and Near-Crashes*; Report No. DOT HS 811 147; National Highway Traffic Safety Administration: Washington, DC, USA, 2009.
9. Cicchino, J.B. Effects of blind spot monitoring systems on police-reported lane-change crashes. *Traffic Inj. Prev.* **2018**, *19*, 615–622. [CrossRef] [PubMed]
10. Das Chakladar, D.; Roy, P.P. *Cognitive Workload Estimation Using Physiological Measures: A Review*; Indian Inst Technol Roorkee, Dept Comp Sci & Engn: Roorkee, India, 2023. [CrossRef]
11. Hart, S.G.; Staveland, L.E. Development of NASA-TLX (Task Load Index): Results of Empirical and Theoretical Research. *Adv. Psychol.* **1988**, *52*, 139–183. [CrossRef]
12. Reid, G.B.; Nygren, T.E. The Subjective Workload Assessment Technique: A scaling procedure for measuring mental workload. *Hum. Ment. Workload* **1988**, *52*, 185–218.
13. Mariel, G.; Elke, V.; von Leupoldt, A.; Mittelstädt, J.M.; Van den Bergh, O. Respiratory Changes in Response to Cognitive Load: A Systematic Review. *Neural Plast.* **2016**, *2016*, 8146809.
14. Veltman, J.A. A Comparative Study of Psychophysiological Reactions during Simulator and Real Flight. *Int. J. Aviat. Psychol.* **2002**, *12*, 33–48. [CrossRef]
15. Palinko, O.; Kun, A.L.; Shyrokov, A.; Heeman, P. Estimating cognitive load using remote eye tracking in a driving simulator. In Proceedings of the Eye-Tracking Research & Applications, Austin, TX, USA, 22–24 March 2010.
16. Prabhakar, G.; Mukhopadhyay, A.; Murthy, L.; Modiksha, M.; Sachin, D.; Biswas, P. Cognitive load estimation using ocular parameters in automotive. *Transp. Eng.* **2020**, *2*, 100008. [CrossRef]
17. Desok, K.; Yunhwan, S.; Hyang-Sook, K.; Jung, S. Short term analysis of long term patterns of heart rate variability in subjects under mental stress. In Proceedings of the 2008 International Conference on BioMedical Engineering and Informatics, Sanya, China, 27–30 May 2008.
18. Andreas, H.; Kati, H.; Anu, H.; Jussi, K.; Kiti, M. Mental workload classification using heart rate metrics. In Proceedings of the 2009 Annual International Conference of the IEEE Engineering in Medicine and Biology Society, Minneapolis, MN, USA, 3–6 September 2009; Annual Conference. IEEE Engineering in Medicine and Biology Society: New York, NY, USA, 2009; Volume 2009, pp. 1836–1839.
19. Boring, M.J.; Ridgeway, K.; Shvartsman, M.; Jonker, T.R. Continuous decoding of cognitive load from electroencephalography reveals task-general and task-specific correlates. *J. Neural Eng.* **2020**, *17*, 056016. [CrossRef]

20. Murtazina, M.; Avdeenko, T. Measuring cognitive load based on EEG data in the intelligent learning systems. In Proceedings of the SLET-2020: International Scientific Conference on Innovative Approaches to the Application of Digital Technologies in Education, Stavropol, Russia, 12–13 November 2020; CEUR Workshop Proceedings: Tenerife, Spain, 2020; Volume 2861, pp. 342–350.
21. Gogna, Y.; Tiwari, S.; Singla, R. Mental Workload Assessment of Gamers' Eeg with Multi-Domain Feature-Based Cognitive Model and Its Validation. *Biomed. Eng. Appl. Basis Commun.* **2024**, *36*, 2450022. [CrossRef]
22. Luque, F.; Armada, V.; Piovano, L.; Barba, R.J.; Santamaría, A. Understanding Pedestrian Cognition Workload in Traffic Environments Using Virtual Reality and Electroencephalography. *Electronics* **2024**, *13*, 1453. [CrossRef]
23. Bulumulle, G.; Boloni, L. A study of the automobile blind-spots' spatial dimensions and angle of orientation on side-sweep accidents. In Proceedings of the 2016 Symposium on Theory of Modeling and Simulation (TMS-DEVS), Pasadena, CA, USA, 3–6 April 2016.
24. Chong, I.; Mirchi, T.; Silva, H.I.; Strybel, T.Z. Auditory and Visual Peripheral Detection Tasks and the Lane Change Test with High and Low Cognitive Load. *Proc. Hum. Factors Ergon. Soc. Annu. Meet.* **2014**, *58*, 2180–2184. [CrossRef]
25. Recarte, M.A.; Nunes, L.M. Mental workload while driving: Effects on visual search, discrimination, and decision making. *J. Exp. Psychol. Appl.* **2003**, *9*, 119–137. [CrossRef] [PubMed]
26. Li, P.; Markkula, G.; Li, Y.; Merat, N. Is improved lane keeping during cognitive load caused by increased physical arousal or gaze concentration toward the road center? *Accid. Anal. Prev.* **2018**, *117*, 65–74. [CrossRef] [PubMed]
27. Melnicuk, V.; Thompson, S.; Jennings, P.; Birrell, S. Effect of cognitive load on drivers' State and task performance during automated driving: Introducing a novel method for determining stabilisation time following take-over of control. *Accident Anal. Prev.* **2021**, *151*, 105967. [CrossRef] [PubMed]
28. Barkana, Y.; Zadok, D.; Morad, Y.; Avni, I. Visual field attention is reduced by concomitant hands-free conversation on a cellular telephone. *Am. J. Ophthalmol.* **2004**, *138*, 347–353. [CrossRef]
29. Seppelt, B.; Seaman, S.; Angell, L.; Mehler, B.; Reimer, B. Differentiating Cognitive Load Using a Modified Version of AttenD. In Proceedings of the Automotive User Interfaces and Interactive Vehicular Applications, Oldenburg, Germany, 24–27 September 2017.
30. Lechner, G.; Fellmann, M.; Festl, A.; Kaiser, C.; Kalayci, T.E.; Spitzer, M.; Stocker, A. A Lightweight Framework for Multi-device Integration and Multi-sensor Fusion to Explore Driver Distraction. In Proceedings of the Advanced Information Systems Engineering: 31st International Conference, CAiSE 2019, Rome, Italy, 3–7 June 2019; Springer International Publishing: Cham, Switzerland, 2019; Volume 11483, pp. 80–95. [CrossRef]
31. Xu, J.; Qian, C.; Han, S.; Guo, F. Detecting Critical Mismatched Driver Visual Attention during Lane Change: An Embedding Kernel Algorithm. In *IEEE Transactions on Intelligent Transportation Systems*; IEEE: New York, NY, USA, 2024; pp. 1–11. [CrossRef]
32. Yuki, M.; Tomonori, O.; Yoshiaki, M.; Daichi, S.; Meiko, M.; Miwa, N. Effects of Placing a CMS Monitor to Present Side and Rear View at the Driver-centered Position on Drivers' Rearward Visual Behavior, Cognitive Load, and Mental Stress. *Int. J. Automot. Eng.* **2022**, *13*, 196–205.
33. Regan, M.; Victor, T.; Lee, J. Chapter 19: The Driver Distraction Detection Algorithm AttenD. In *Driver Distraction and Inattention*; Advances in Research and Countermeasures; CRC Press: Boca Raton, FL, USA, 2013; Volume 1.
34. Iddrisu, W.A.; Gyabaah, O. Identifying factors associated with child malnutrition in Ghana: A cross-sectional study using Bayesian multilevel ordinal logistic regression approach. *BMJ Open* **2023**, *13*, e075723. [CrossRef]
35. Soda, M.A.; Hamuli, E.K.; Batina, S.A.; Kandala, N.-B. Determinants and spatial factors of anemia in women of reproductive age in Democratic Republic of Congo (drc): A Bayesian multilevel ordinal logistic regression model approach. *BMC Public Health* **2024**, *24*, 202. [CrossRef] [PubMed]
36. Montesinos-López, O.A.; Montesinos-López, A.; Crossa, J.; Burgueño, J.; Eskridge, K. Genomic-Enabled Prediction of Ordinal Data with Bayesian Logistic Ordinal Regression. *G3 Genes Genomes Genet.* **2015**, *5*, 2113–2126. [CrossRef] [PubMed]
37. Gianola, D.; Foulley, J. Sire evaluation for ordered categorical data with a threshold model. *Genet. Sel. Evol.* **1983**, *15*, 201–224. [CrossRef]
38. Zhiwen, G.; Sheng, F.; Changchang, M.; Kai, W.; Kan, H.; Weijie, Z.; Xiaojun, D.; Lufang, F.; Jinghao, H. Quantifying and comparing the effects of key chemical descriptors on metal–organic frameworks water stability with CatBoost and SHAP. *Microchem. J.* **2024**, *196*, 109625.
39. Zahid, M.; Habib, M.F.; Ijaz, M.; Ameer, I.; Ullah, I.; Ahmed, T.; He, Z. Factors affecting injury severity in motorcycle crashes: Different age groups analysis using Catboost and SHAP techniques. *Traffic Inj. Prev.* **2024**, *25*, 472–481. [CrossRef]
40. Yao, Z.; Chen, M.; Zhan, J.; Zhuang, J.; Sun, Y.; Yu, Q.; Yu, Z. Refined Landslide Susceptibility Mapping by Integrating the SHAP-CatBoost Model and InSAR Observations: A Case Study of Lishui, Southern China. *Appl. Sci.* **2023**, *13*, 12817. [CrossRef]
41. Prokhorenkova, L.; Gusev, G.; Vorobev, A.; Dorogush, A.V.; Gulin, A. CatBoost: Unbiased boosting with categorical features. *Adv. Neural Inf. Process. Syst.* **2019**, *31*. [CrossRef]
42. Dureckova, H.; Krykunov, M.; Aghaji, M.Z.; Woo, T.K. Robust Machine Learning Models for Predicting High CO_2 Working Capacity and CO_2/H_2 Selectivity of Gas Adsorption in Metal Organic Frameworks for Precombustion Carbon Capture. *J. Phys. Chem. C* **2019**, *123*, 4133–4139. [CrossRef]

43. Lundberg, S.; Lee, S.-I. A unified approach to interpreting model predictions. In Proceedings of the 2017 Neural Information Processing Systems (NIPS) Conference, Long Beach, CA, USA, 4–9 December 2017.
44. Szumska, E.M.; Grabski, P.T. An analysis of the impact of the driver's height on their visual field range. In Proceedings of the 2018 XI International Science-Technical Conference Automotive Safety, Casta, Slovakia, 18–20 April 2018.

Disclaimer/Publisher's Note: The statements, opinions and data contained in all publications are solely those of the individual author(s) and contributor(s) and not of MDPI and/or the editor(s). MDPI and/or the editor(s) disclaim responsibility for any injury to people or property resulting from any ideas, methods, instructions or products referred to in the content.